

Modeling retinal electrical stimulation

Victor Amiot, Raphael Ausilio, Andy Bonnetto, Valentin Karam, Tanguy Roche

Abstract—Retinal prostheses are a promising solution for vision recovery in patients suffering from a loss of photoreceptors as it is the case in diseases such as age-related macular degeneration (AMD) and retinitis pigmentosa (RP). They are however limited in performance due to the intricacy of the retinal network which lacks knowledge and understanding. In this context, we considered the problem of determining the complex retinal behaviour under electrical stimulation. We proposed the cascade of two existing models respectively based on finite element modeling (FEM) to simulate the current injection by an electrode, and on a biophysically-inspired neuronal network. Simulation parameters for the retina degeneration state and the electrical pulses were determined, before presenting a potential set-up for electrical stimulation relying on an array of 3×3 electrodes. Results showed in a first place the exact replication of our model with previous work [1], both with light and electrical stimulation. Then, we addressed a specific case with degenerated photoreceptors and bipolar cells, and we proposed a framework to optimize existing devices. It consists in modifying the electrode current to recover a normal value for the ganglion cells firing rate that approaches a healthy retinal state. Future perspectives for this model were addressed such as its implementation in a bigger framework from the patient retina state recording to the generation of personalized current protocols.

Index Terms—Retinal implant, Retinal stimulation, Electrical stimulation, Retinal degeneration, Retinal modeling.

I. INTRODUCTION

Light radiation from the external world is focused on the retina by eye structures, transduced into electrical signals by photoreceptors, processed by the retinal network including horizontal, bipolar, amacrine and ganglion cells, and transmitted to the visual cortex via the optic nerve. However, this information flow can be hindered by diseases such as age-related macular degeneration (AMD) and retinitis pigmentosa (RP), which are both responsible for the loss of photoreceptors in the retina, in the center and in the periphery respectively (Fig. 9) [2]. On one hand, AMD is a progressive disease that affects 300 000 new people yearly in the US among which 10% result in complete blindness [3], while RP is a genetic disease with 1/4000 prevalence worldwide [3]. Given that no treatment is available in AMD while RP requires early therapy to prevent the loss of photoreceptors, both diseases may lead to blindness.

As a solution, visual prostheses have been studied at the three levels of cortex, optic nerve, and retina [3]. However, because of the invasiveness and the high complexity of the two first ones, only retinal prostheses are currently commercially available. Depending on their implant location in the retina, they can be divided into suprachoroidal, epiretinal, or subretinal. The highest visual acuity currently achieved for these

three types of prostheses is, respectively, < 20/4451, 20/1260 and 20/546, thus below the 20/200 sufficient to define a patient as legally blind in the US and very far from the able-sighted acuity of 20/20 [2, 4].

Hybrid neural – finite element models have been used in the past to optimize neural interfaces with the peripheral nervous system [5, 6] and could improve the temporal and spatial selectivity of retinal implants. Currently, Cottaris and Elfar (2005) [1] proposed a biophysically-inspired neuronal network model of the retina involving nine cell types, which can be stimulated through light and electrical pulses. Instead, in Joarder et al. (2011) [7], a Finite element modeling (FEM) framework for the detailed computation of the potential distribution due to retinal electrical stimulation has been developed. While the former model does not consider the inhomogeneous electrical conductivity of retina tissues, the second one neglects the complex neural dynamics occurring in the retina. To the best of our knowledge, no attempt has been made to combine FEM with a biophysical model of the retinal network that could provide a more complete description of retinal behaviour under electrical stimulation. Finally, while Cottaris and Elfar (2005) [1] allow for photoreceptor degeneration, this phenomenon accurately describes only the early stages of the target diseases. Here we address a more severe degeneration pattern, where the bipolar cell transmission is compromised as well, as observed by Marc et al. (2003) [8]. A framework of the model to optimize existing devices is thus presented, where electrical stimulation is tuned to approach the same retinal ganglion cells firing rate as in a healthy retina.

II. METHODS

A. Finite element modeling

The FEM part has been created in *COMSOL multiphysics*, and then the *COMSOL with Matlab* software allowed us to automatize the model creation process.

This retinal FEM geometry is composed of a stack of nine passive layers (Fig. 1), each having a specific electrical conductivity. These conductivities have been taken from Joarder et al. (2011) [7]. Current was injected by an electrode at a specific depth, depending on whether an epiretinal, subretinal, or suprachoroidal stimulation is simulated. The output is a 3D stationary scalar field of the voltage at any point. Resistive potential drops (ΔV_e) are calculated from the interpolation of the voltage field at each cellular location and injected in the temporal model (Fig. 10 in Appendix).

B. Spatiotemporal model

The spatiotemporal model is a replica of Cottaris and Elfar (2005) work in Matlab [1].

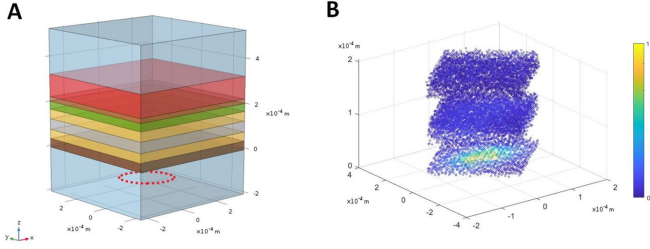


Fig. 1. (A) FEM model composed of 9 layers, with the position of the electrode marked by the red dotted lines in epiretinal case (B) Normalised potential drops mean values (ΔV_e) of voltage differences on opposite point couples for each cell in epiretinal case.

1) *Spatial model:* The spatial part of the model is separated into the generation of retina cells position in 3D space and the formation of excitatory and inhibitory connections between neurons. Neurons considered are classified in 9 different types: cone photoreceptors (CR), horizontal cells (HRZ), ON and OFF bipolar cells (BP_{on} and BP_{off}), ON and OFF wide field amacrine cells (AM^{WF}_{on} and AM^{WF}_{off}), ON narrow field amacrine cells (AM^{NF}_{on}) and ON and OFF ganglion cells (GL_{on} and GL_{off}). These neurons were placed on a 2D lattice with spacings adapted to their types. Cells were then randomly affiliated to a z position using a uniform distribution with ranges depending on their type (Fig. 12 and 13 in Appendix).

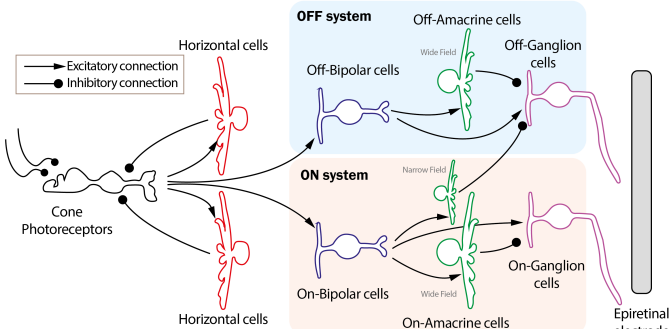


Fig. 2. Connection diagram between cell types, reproduced from [1].

Connections between cells were defined based on their type-dependent dendritic tree extensions. Only connections respecting the reference diagram were represented (Fig. 2).

2) *Temporal model:* Membrane potentials (V_m) evolution over time of all cells were computed under light stimulation and electrical stimulation. They are determined for each cell by their synapses conductances (G_{syn}) changing over time, the cell conductance (G_m) and the ΔV_e matrix driven by the electrodes as shown in the first order differential equation (1).

$$\begin{aligned} \tau_m \frac{dV_m}{dt} &= -V_m(t) + V_s(t) \\ V_s(t) &= \frac{1}{G_{total}(t)} [G_m(E_{rest} + \Delta V_e) + \sum_{syn} G_{syn}(t) E_{syn}] \end{aligned} \quad (1)$$

The synapse conductances are determined by internal parameters related to the cells types of connection, the distance between cell somas and V_m of the post synaptic neuron at a

time $t - \tau_{syn}$ where τ_{syn} is a delay equal to 1ms. Everything is described in equation (2) in Appendix. Precise information on the parameter values can be found in the paper of Cottaris and Elfar (2005) [1].

In order to compare our model with the reference article, we stimulated the cells with the same light protocols and electrical protocols. During electrical stimulation, CR cells and HRZ cells are completely degenerated as they made the assumption of total photoreceptor degeneration. HRZ cells being only connected to CR, they would not have any influence on the simulation.

C. Simulation parameters

In order to create currents which would compensate for the degeneration of other cells than CR cells, we focused on a case where additionally to CR cells, BP cells are also degenerated. As displayed in Fig. 3, we induced a Gaussian degeneration of BP cells from both ON and OFF type and used an electrode of 40 μ m diameter. Upon electrode stimulation we expect changes of GL cells firing rate at the location of the degeneration compared to a setup where no BP cells are degenerated. For this simulation we chose pulses lasting 30ms and ranging from 400 μ A to 700 μ A since it corresponds the most to GL cells reaction to a full intensity of light in terms of V_m variations.

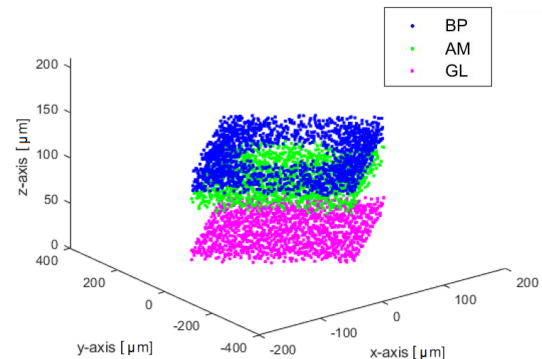


Fig. 3. Spatial configuration of cells without CR and HRZ cells, and with Gaussian BP cell degeneration.

D. Multiple electrode simulation

In order to test different electrode configurations in a reasonable time, we have developed a model based on the superposition of potentials, and took advantage of the uniform nature of retina on the horizontal plane.

We implemented a 3×3 electrodes configuration on the same cellular configuration as in the previous simulation. Electrode diameters were reduced to 10 μ m diameter to maintain the 3×3 matrix in the same size range as the single electrode [9] and each electrode current was divided by 10 compared to the previous setup. In this experiment we try to manually tune currents for compensating BP cell degeneration by changing the ratio of the middle electrode current intensity with respect to the one from the surrounding electrodes. Ratios from -2 to 4 were tested and the visual aspect of the obtained distribution of potential can be seen in

Fig. 4 for a ratio of 4.

Superposition: In order to speed computations up, a superposition method has been implemented, allowing the FEM to be computed with one single electrode on a small retina portion. The potential matrix created by this single electrode is scaled and shifted to represent each other electrode and summed, allowing to create large multi-electrodes patterns in very short time compared to other methods (Fig. 11). In this regard, our method becomes particularly advantageous when scaling the number of electrodes.

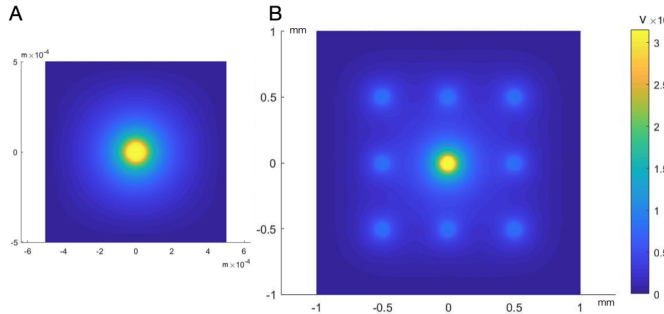


Fig. 4. 2D Z-Slice of the resulting potential field. (A) unitary 1x1 mm patch before superposition. (B) 3 × 3 electrodes array created by superposition of the patch with a ratio of 4 between central and surrounding electrodes (*Here the input current of the middle electrode is 1A*).

III. RESULTS

A. Model replication

The first results shown compare our model responses to light and electrical stimulation with the ones from the reference article [1].

1) *Light stimulation:* Fig. 5 shows variations of V_m for all types of cells after four 80 μ m diameter disk-shaped pulses of normalized light contrasts with sequentially 1,0.4,-0.4 and -1 intensities.

2) *Electrical stimulation:* Additionally, we compared the response of our model to electrical pulses coming from a single electrode with a diameter of 80 μ m (Fig. 6).

The results for simulation with electrical pulses replicating the reference paper are shown in Fig. 6.

B. Electrical stimulation with bipolar cell degeneration

Fig. 7 shows the average normalized firing rates with and without BP cells degeneration after removing edge effects. Edge effects happen because a smaller electrode is used in this simulation setup. We estimated the average firing rate to be a good approximation considering the small size of the retina patch simulated.

C. Multiple electrodes stimulation

In the case of multiple electrodes stimulation with degenerated BP cells as shown in Fig. 3, we tried to manually adapt the value of the current produced by each electrode in order to compensate for the Gaussian degeneration of the cells. As shown in Fig. 8, we notice a slight difference in depolarization

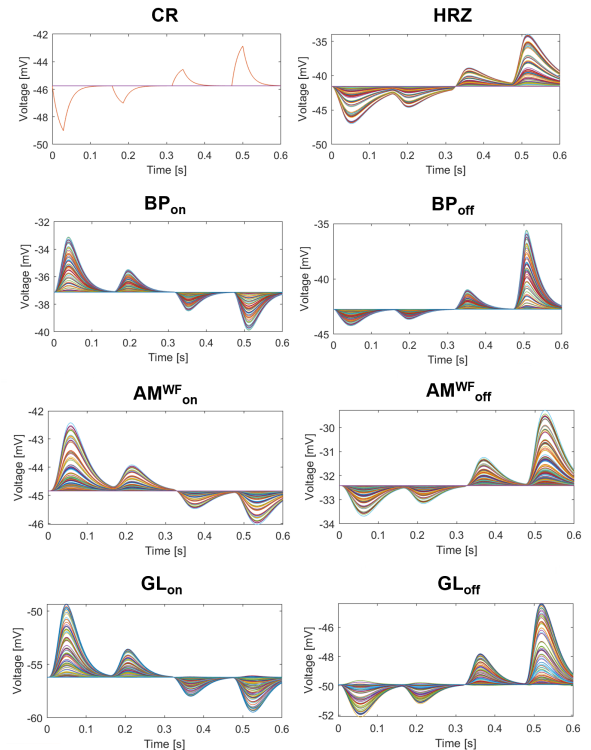


Fig. 5. Membrane potentials for each cell type under light pulses stimulation (Normalized light intensity contrast = [1,0.4,-0.4-1]), not shown AM^{WF}_{on} cells for practical display (Fig. 14 in Appendix).

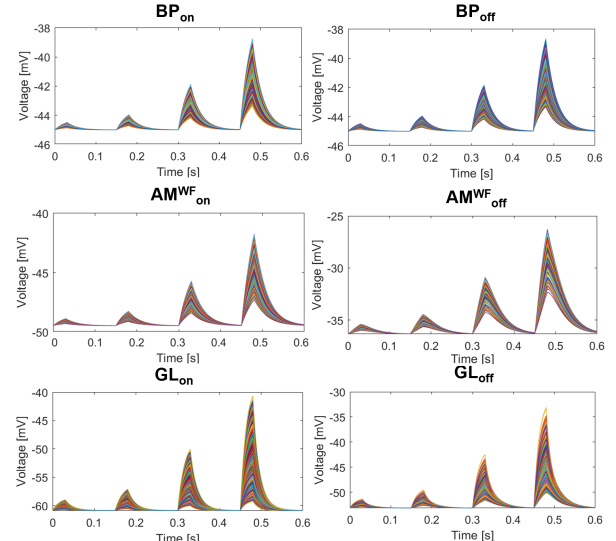


Fig. 6. Membrane potentials for each cell type under electrical pulse stimulation (pulse intensity = [75 μ A, 150 μ A, 300 μ A, 600 μ A]), not shown AM^{WF}_{on} cells for practical display (Fig. 14 in Appendix).

of GL_{on} cells between the stimulation with the array where all electrodes inject the same current, compared to the array where the central electrode injects more current, however this difference is not significant.

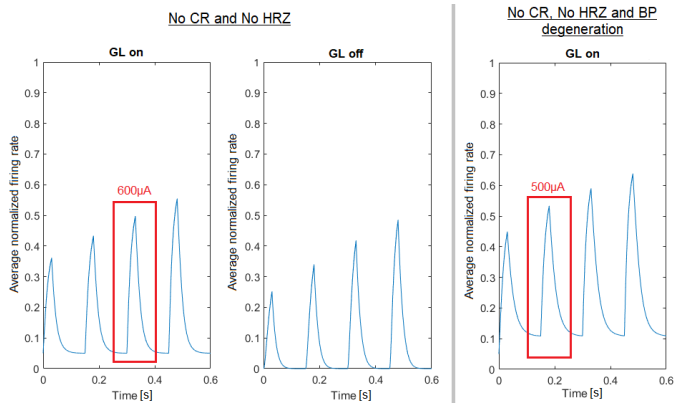


Fig. 7. Average normalized firing rates for GL_{on} and GL_{off} cells during electrical stimulation, (left) without BP cell degeneration, (right) with BP cell degeneration. GL_{off} showed no firing rate at all upon electrical stimulation after BP cell degeneration.

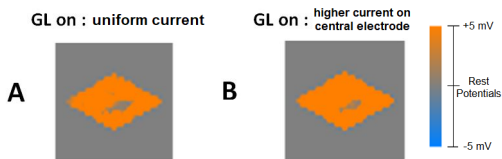


Fig. 8. (A) V_m of the GL_{on} layer in the case where the nine electrodes of the 3×3 matrix injects a uniform current, (B) V_m of the GL_{on} layer in the case where the central electrode injects 4 times more current than the surrounding electrodes.

IV. DISCUSSION AND CONCLUSION

Light and electrical simulation give analog results of V_m in terms of waveform with respect to space and time compared to the reference article [1]. Further model optimization would be needed to correct for eventual variations.

On the simulation setup, GL_{on} cells are depolarized whereas GL_{off} cells appeared to be highly hyperpolarized on the center of the lattice where BP cell degeneration occurs (Fig. 15 in Appendix). By comparing the average normalized firing rates, we observe an increase of around 10% for the GL_{on} cells firing rate and a huge decrease of GL_{off} firing rate (not shown) down to 0% upon BP degeneration. According to this result, it would be possible to compensate up to a certain degree for BP degeneration only for GL_{on} cells by decreasing the current injected in the single electrode. For instance, a current of 600 μ A (third pulse) in a retina without BP cell degeneration has a similar GL_{on} average normalized firing rate than a current of 500 μ A in a retina with BP cell degeneration. Hyperpolarization of the GL_{off} is advanced and may relate to the dominance of light perception over dark perception during electrical stimulation [10]. Further studies can be done on the degeneration at various degrees and with other cell types.

Concerning the stimulation by a 3×3 matrix, where the current was manually tuned, it seems, in view of the inconclusive results, that choosing the current injected by each electrode cannot be done in such a simplistic way. The electric field produced by a matrix of electrodes is complex and not intuitive. As the potential fields produced by each electrode

are not sufficiently localised, they superimposed and spread out along with the increase of the distance from the electrode surface.

Local return would allow more localization of the electric field produced by each electrode as studied by Fan et al (2019) [9]. A modification of the FEM model could easily be made to include these returns, which would also allow the study of cell stimulation at the individual level, an eventual solution to the problem of simultaneous activation of ON and OFF pathways.

The validation of this model should be assessed with physiological recording of GL cells *in vivo* which may recommend advances in the state of the art.

We propose a strategy to use this computational framework from the patient retina state recording to the generation of personalized current protocols (Fig. 16 in Appendix). From the cellular spatial configuration, an electrode matrix and a fitting algorithm, we would be able to produce a patient specific current pattern to be added to the traditional non patient-specific current protocols. The fitting algorithm would find the best current protocol by reducing the error as the difference between a stimulated retina with complex degeneration patterns and a retina with only photoreceptor degeneration. This part has recently been covered by Shah et al. [11] with a Greedy Algorithm but could also be done with machine learning algorithms.

The implementation and optimization of the FEM system is highly compatible with the dataset generation of the fitting algorithm. In other hand, the main limitation of the spatiotemporal system for modeling full prosthesis area is its slowness. Conceptually, it solves first order differential equation for each cell sequentially in time which makes it hardly scalable. Modifications of the equations to cover larger surfaces with less cell density is difficult without introducing significant variations of equilibrium points. A higher effective surface would allow the possibility to study phosphene elongation phenomenon [12]. Another approach would be to use spiking neural network to model the cells dynamics [13].

During this project, we were able to replicate an electrical retinal stimulation model through the use of two major pipelines. First, we considered the retina as a stack of purely resistive layers, to which we shaped a voltage pattern through an electrode array. Then, we considered the connections between the layers of cells, allowing us to transform this stationary map into a spatiotemporal model. We were able to simulate the output firing rates under light and electrical stimulation for multiple conditions, including photoreceptors and bipolar cells degeneration. Finally, we were able to show that the compensation for the loss of bipolar cells by tuning the electrode current is partially possible using this model. In future prospects, we should combine this computational framework with machine learning algorithms to optimize the current generation and propose personalized therapy for each individual pathology.

REFERENCES

- [1] Nicolas P Cottaris and Sylvia D Elfar. How the retinal network reacts to epiretinal stimulation to form the prosthetic visual input to the cortex. *Journal of Neural Engineering*, 2(1):S74–S90, Feb 2005. doi: 10.1088/1741-2560/2/1/010.
- [2] G. A. Goetz and D. V. Palanker. Electronic approaches to restoration of sight. *Reports on Progress in Physics*, 79(9):096701, Aug 2016. ISSN 0034-4885. doi: 10.1088/0034-4885/79/9/096701. Publisher: IOP Publishing.
- [3] Rodrigo A. Brant Fernandes, Bruno Diniz, Ramiro Ribeiro, and Mark Humayun. Artificial vision through neuronal stimulation. *Neuroscience Letters*, 519(2):122–128, June 2012. ISSN 0304-3940. doi: 10.1016/j.neulet.2012.01.063.
- [4] Wei Tong, Hamish Meffin, David J. Garrett, and Michael R. Ibbotson. Stimulation Strategies for Improving the Resolution of Retinal Prostheses. *Frontiers in Neuroscience*, 14:262, 2020. ISSN 1662-453X. doi: 10.3389/fnins.2020.00262.
- [5] Simone Romeni, Giacomo Valle, Alberto Mazzoni, and Silvestro Micera. Tutorial: a computational framework for the design and optimization of peripheral neural interfaces. *Nature Protocols*, 15(10):3129–3153, October 2020. ISSN 1750-2799. doi: 10.1038/s41596-020-0377-6.
- [6] Eduardo Martin Moraud, Marco Capogrosso, Emanuele Formento, Nikolaus Wenger, Jack DiGiovanna, Grégoire Courtine, and Silvestro Micera. Mechanisms Underlying the Neuromodulation of Spinal Circuits for Correcting Gait and Balance Deficits after Spinal Cord Injury. *Neuron*, 89(4):814–828, February 2016. ISSN 1097-4199. doi: 10.1016/j.neuron.2016.01.009.
- [7] Saiful A Joarder, Miganooosh Abramian, Gregg J Suaning, Nigel H Lovell, and Socrates Dokos. A continuum model of retinal electrical stimulation. 8(6):13pp, Oct 2011. doi: 10.1088/1741-2560/8/6/066006.
- [8] Robert E Marc, Bryan W Jones, Carl B Watt, and Enrica Strettoi. Neural remodeling in retinal degeneration. *Progress in Retinal and Eye Research*, 22(5):607–655, September 2003. ISSN 1350-9462. doi: 10.1016/S1350-9462(03)00039-9.
- [9] Victoria Fan, Lauren Grosberg, Sasidhar Madugula, Pawel Hottowy, Wladyslaw Dabrowski, Alexander Sher, Alan Litke, and Chichilnisky. Epiretinal stimulation with local returns enhances selectivity at cellular resolution. *J. Neural Eng.*, 2019. ISSN 1741-2552. doi: 10.1088/1741-2552/aaeef1.
- [10] James Golden, Cordelia Erickson-Davis, Nicolas Cottaris, Nikhil Parthasarathy, Fred Rieke, David Brainard, Brian Wandell, and E Chichilnisky. Simulation of visual perception and learning with a retinal prosthesis. *J. Neural Eng.*, 2019. ISSN 1741-2552. doi: 10.1088/1741-2552/aaf270.
- [11] Nishal P. Shah, Sasidhar Madugula, Lauren Grosberg, Gonzalo Mena, Pulkit Tandon, Pawel Hottowy, Alexander Sher, Alan Litke, Subhasish Mitra, and E.J. Chichilnisky. Optimization of electrical stimulation for a high-fidelity artificial retina. In *2019 9th International IEEE/EMBS Conference on Neural Engineering (NER)*, pages 714–718, 2019. doi: 10.1109/NER.2019.8716987.
- [12] Wei Tong, Hamish Meffin, David J. Garrett, and Michael R. Ibbotson. Stimulation strategies for improving the resolution of retinal prostheses. *Frontiers in Neuroscience*, 14:262, 2020. ISSN 1662-453X. doi: 10.3389/fnins.2020.00262.
- [13] Kyle Loizos, Robert E. Marc, Mark S. Humayun, James R. Anderson, Bryan W. Jones, and Gianluca Lazzi. Increasing electrical stimulation efficacy in degenerated retina: Stimulus waveform design in a multiscale computational model. *IEEE Transactions on Neural Systems and Rehabilitation Engineering*, 26:1111–1120, 2018.

V. APPENDIX

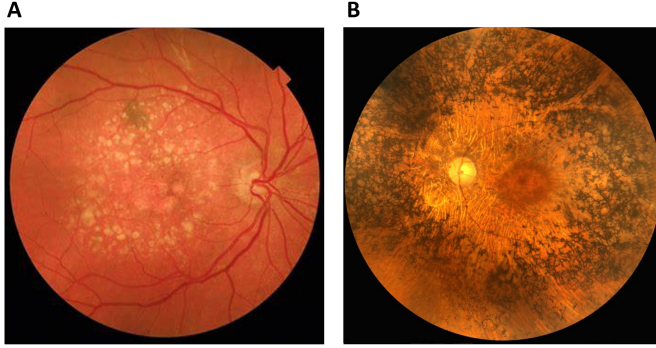


Fig. 9. Photographs of the retina affected by (A) age-related macular degeneration (AMD) showing a loss of photoreceptors in the center and (B) retinitis pigmentosa (RP) showing a loss of photoreceptors in the periphery.

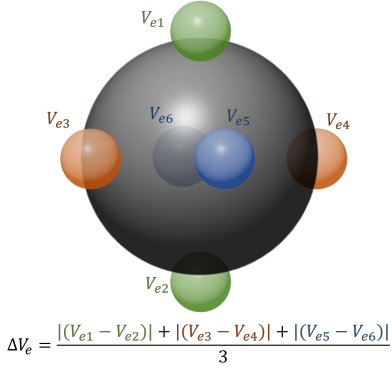


Fig. 10. Calculation of the resistive potential drop for a given cell by taking the mean value of potential field difference at six opposite points couples.

Equations for synaptic conductance at time t:

$$G_{syn,i} = \frac{1}{W} \sum_j g_{syn,i,j}(t) \exp\left(-\frac{D_{i,j}}{\sigma_i}\right)$$

$$g_{syn,i,j=I}(t) = g_{min,i} + (g_{max,i} - g_{min,i}) [1 - (1 + \exp(\frac{V_{m,j}(t - \tau_{syn} - V_{50,i})}{\beta_i}))^{-1}]$$

$$g_{syn,i,j=D}(t) = g_{min,i} + (g_{max,i} - g_{min,i}) [1 - (1 + \exp(\frac{V_{m,j}(t - \tau_{syn} - V_{50,i})}{\beta_i}))^{-1}]$$

$$W = \sum_j \exp(-\frac{D_{i,j}}{\sigma_i})$$
(2)

Theoretical computation time equation for a model computed with Standard Superposition, compared with our Patch Superposition Method. The FEM processing time is t_{FEM} , and the matrix superposition timing is t_{Sup} :

$$t_{Stand.Sup.} = K * ((N * N * t_{FEM1}) + (M * t_{Sup1}))$$

$$t_{PatchSup.} = t_{FEM2} + K * (M * t_{Sup2})$$
(3)

N : Number of electrodes

M : Number of iterations (current values)

K : Number of electrode configurations

	Standard Sup.	Patch Sup.	Standard Sup.	Patch Sup.
Number of electrodes N	1600	20	480	40
t_{FEM} (s)	120	20	480	40
t_{Sup} (s)	78	50	720	165
For 1 current config. (s)	//	1,92078E+05	70	3,07272E+06
For M different currents (s)	100	1,998E+05	5,02E+03	3,144E+06
For K electrode config. (s)	1000	1,998E+08	5,0E+06	3,144E+09
Ratio of timings		40		190,5

Fig. 11. Table summarizing the timing we had, using the classical superposition compared with our patch superposition. The top table gathers our measurement made with our personal computers, the middle table applies the equation (3) to our data (first for M currents only, and then adding K electrode configurations), and the bottom table performs the ratio between the standard superposition timings and the patch superposition timings (taking into account the K and M parameters).

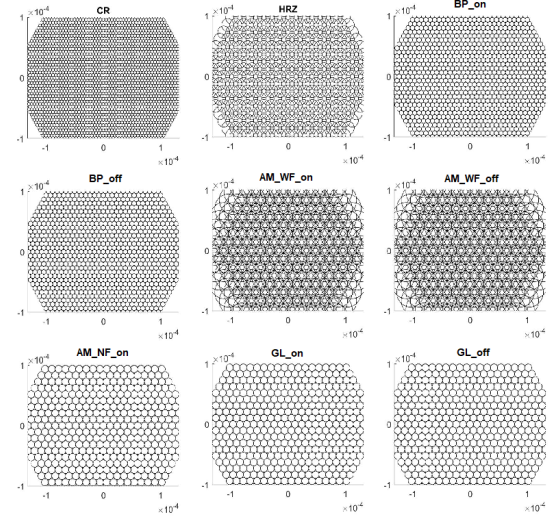


Fig. 12. Cell lattices with cell positions and dendritic tree diameters per cell type with no lateral spatial noise, axes units are in meter.

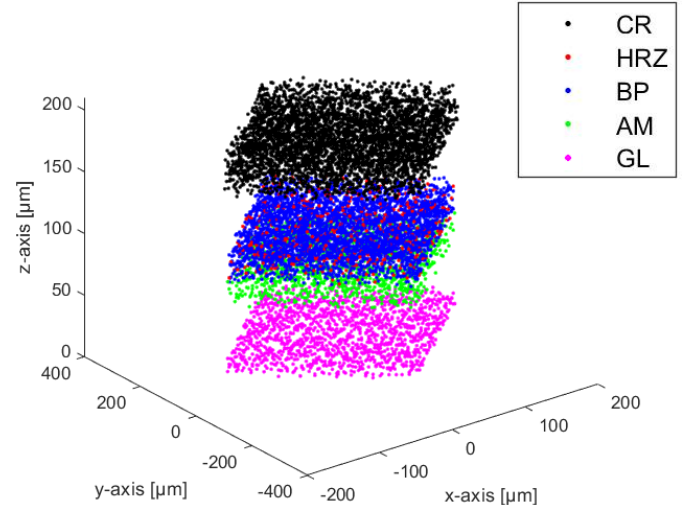


Fig. 13. 3D representation of all cells per cell type.

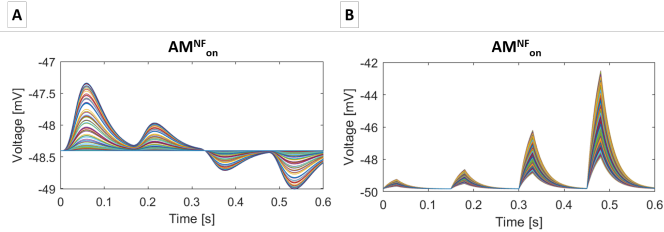


Fig. 14. Membrane potential for AM^{NF}_{on} cells under (A) light stimulation and (B) electrical stimulation.

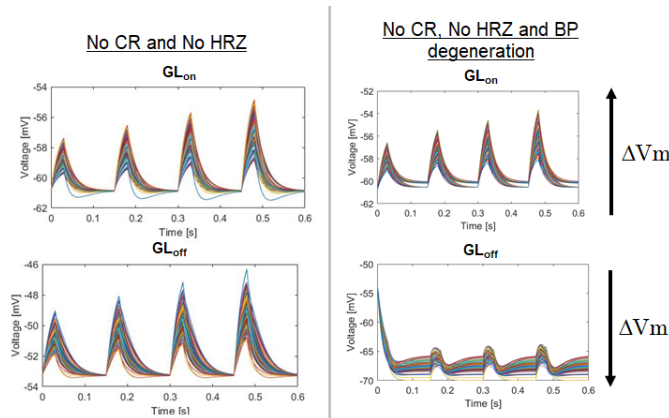


Fig. 15. Membrane potentials for GL_{on} and GL_{off} cells during electrical stimulation, (left) without BP cell degeneration, (right) with BP cell degeneration. GL_{off} showed no firing rate at all upon electrical stimulation after BP cell degeneration.

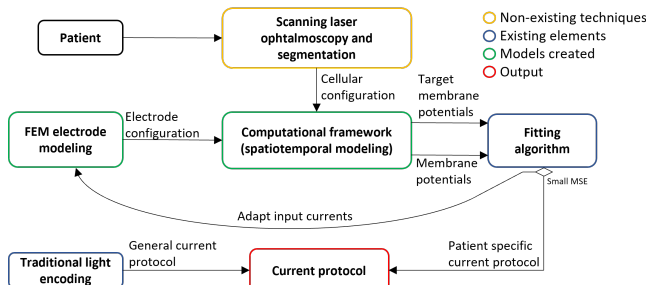


Fig. 16. Use of the computational framework in a patient specific application.